Magnetic Anomaly Detection Using a Three-Axis Magnetometer

5 authors, including:

Boris Ginzburg
Soreq Nuclear Research Center
22 PUBLICATIONS   **365** CITATIONS

Magnetic Anomaly Detection Using a Three-Axis Magnetometer

Arie Sheinker[1,2], Lev Frumkis[2], Boris Ginzburg[1], Nizan Salomonski[1], and Ben-Zion Kaplan[2]

[1]R&D Integrated Systems Section, Propulsion Division, SOREQ NRC, Yanve 81800, Israel
[2]Department of Electrical and Computer Engineering, Ben-Gurion University of the Negev, Beer-Sheva 84105, Israel

Magnetic anomaly detection is a good method for detecting ferromagnetic objects, particularly hidden targets. In this work, we address the detection of a moving ferromagnetic target using a static three-axis referenced magnetometer. The analysis and the results are also applicable to the converse case of a static ferromagnetic target and a moving three-axis referenced magnetometer. We use the three magnetometer outputs to build a total magnetic field of the target. This signal is decomposed into a set of orthonormal basis functions, out of which the dominant basis function is chosen as the detector. The detector provides output responses to any target magnetic moment orientation. We support the analysis by a computer simulation and real-world experimental results. The high detection probability and the simple implementation of the proposed method make it attractive for real-time applications.

Index Terms—**Magnetic anomaly detection (MAD), orthonormal basis functions, three-axis referenced magnetometer.**

I. INTRODUCTION

MAGNETIC ANOMALY DETECTION (MAD) has been used for decades to detect ferromagnetic targets. The static magnetic field is indifferent to weather conditions. Moreover, air, water, and most soils are practically transparent to the static magnetic field, which makes MAD especially attractive for detecting hidden targets [1]. As a passive method, MAD has an advantage over other techniques [2] in staying unrevealed by the target. Several applications have been developed to detect a target by exploiting the magnetic anomaly it produces in the ambient earth magnetic field [3], [4]. A ferromagnetic target generates a magnetic field, $\vec{B}$, which in many cases can be modeled using a multipole model [5]. At distances more than three times the target largest dimension, it is a common practice to treat its magnetic field as being produced by a point magnetic dipole [1], [3]. Since in this work we are interested in remote sensing with long detection range, we will adopt the point magnetic dipole field model for the far field [6]

$$\vec{B}(\vec{m}, \vec{r}) = \frac{\mu_0}{4\pi} \left[\frac{3(\vec{m} \cdot \vec{r})\vec{r}}{|\vec{r}|^5} - \frac{\vec{m}}{|\vec{r}|^3} \right]. \tag{1}$$

The target magnetic moment is denoted by $\vec{m} = m_x\hat{x} + m_y\hat{y} + m_z\hat{z}$, where $\hat{x}, \hat{y}, \hat{z}$ are the unit vectors in the Cartesian coordinate frame. The distance between the target and the sensor is $\vec{r}$, and μ_0 is the permeability of air. A magnetic sensor [7], [8] measures a net field composed of the target magnetic induction field, the earth magnetic field, and magnetic noise. In this work, we address the detection of a moving ferromagnetic target by a static three-axis referenced magnetometer. This case is suitable for applications such as intruder detection [9], car traffic monitoring [10], systems to halt runway crashes by detecting traffic on a runway, just to mention a few. Nevertheless, the mathematical analysis and the results are also applicable to the case of a static target and a moving three-axis referenced magnetometer [11]. We use the three magnetometer outputs to build a total magnetic field of the target. This signal is decomposed into a set of orthonormal basis functions (OBFs) [12], out of which the dominant OBF is chosen as the detector. The detector output responses to any target magnetic moment orientation. The analytical results are supported by a computer simulation and a real-world experiment.

II. PROBLEM FORMULATION

Consider a magnetic measurement system which consists of a pair of three-axis magnetometers. One magnetometer is placed at the origin in order to detect the target, whereas the other is used as a reference. For effective differential operation, the reference magnetometer should not sense the target and therefore it is placed far enough from the origin. Both magnetometers are aligned in the same direction, thus, reference readings are subtracted axis by axis from the readings of the magnetometer at the origin. In this manner, the earth magnetic field is canceled and common external interferences of far origin are rejected. In many cases, differential measurements enhance the SNR, although the noise is larger than a single magnetometer intrinsic noise by a factor of $\sqrt{2}$.

The ferromagnetic target is assumed to move with a constant velocity v along a straight line track as is depicted in Fig. 1. We also assume that the target magnetic moment magnitude and orientation are constant in the vicinity of the magnetometer. We chose a Cartesian coordinate frame where $\hat{x}$ is a unit vector starting at the origin and parallel to the target track. The unit vector $\hat{y}$ starts at the origin and is perpendicular to the target track. The unit vector $\hat{z}$ is defined according to right-hand coordinate system. The target track is expressed as a function of time t by

$$\vec{r}(t) = v \cdot t \cdot \hat{x} + R_0 \cdot \hat{y}. \tag{2}$$

At time $t = 0$ the mobile magnetometer passes by the target at a closest proximity approach (CPA) of R_0. In this case we
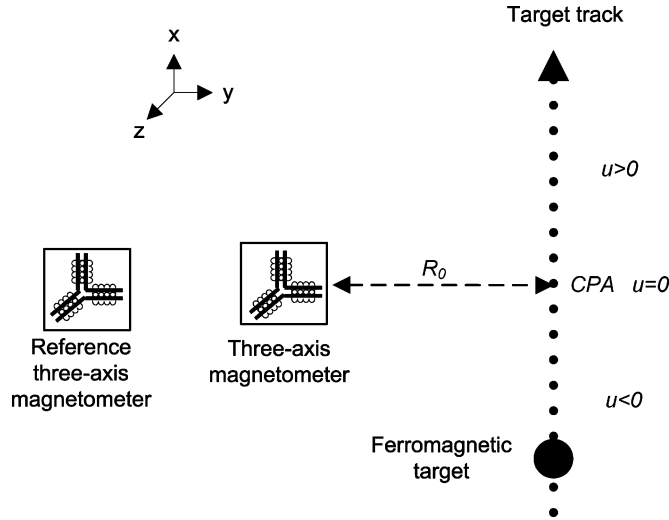
Fig. 1. Three-axis referenced magnetometer detects a ferromagnetic target that moves along a straight line track with a constant velocity.

can describe the target location using a single dimensionless variable u, where u is defined as the position of the target along the track by

$$u = \frac{vt}{R_0}. \qquad (3)$$

Substituting for u yields

$$\vec{r}(u) = u \cdot R_0 \cdot \hat{x} + R_0 \cdot \hat{y}. \qquad (4)$$

By substituting (4) into (1), we get the expression for the produced magnetic induction field as function of a single variable u and the parameters R_0, m_x, m_y, and m_z

$$\vec{B}(u) = \frac{\mu_0}{4\pi R_0^3} \left[\frac{3m_x u^2}{(u^2+1)^{2.5}} + \frac{3m_y u}{(u^2+1)^{2.5}} - \frac{m_x}{(u^2+1)^{1.5}} \right] \cdot \hat{x}$$
$$+ \frac{\mu_0}{4\pi R_0^3} \left[\frac{3m_x u}{(u^2+1)^{2.5}} + \frac{3m_y}{(u^2+1)^{2.5}} - \frac{m_y}{(u^2+1)^{1.5}} \right] \cdot \hat{y}$$
$$- \frac{\mu_0}{4\pi R_0^3} \left[\frac{m_z}{(u^2+1)^{1.5}} \right] \cdot \hat{z}. \qquad (5)$$

The earth magnetic field and other external magnetic interferences were ignored since they are canceled by the differential measurements. Using $u^2(u^2+1)^{-2.5} + (u^2+1)^{-2.5} = (u^2+1)^{-1.5}$ we rewrite (5)

$$\vec{B}(u) = \frac{\mu_0}{4\pi R_0^3} \left[\frac{2m_x u^2}{(u^2+1)^{2.5}} + \frac{3m_y u}{(u^2+1)^{2.5}} - \frac{m_x}{(u^2+1)^{2.5}} \right] \cdot \hat{x}$$
$$+ \frac{\mu_0}{4\pi R_0^3} \left[-\frac{m_y u^2}{(u^2+1)^{2.5}} + \frac{3m_x u}{(u^2+1)^{2.5}} + \frac{2m_y}{(u^2+1)^{2.5}} \right] \cdot \hat{y}$$
$$- \frac{\mu_0}{4\pi R_0^3} \left[\frac{m_z u^2}{(u^2+1)^{2.5}} + \frac{m_z}{(u^2+1)^{2.5}} \right] \cdot \hat{z}. \qquad (6)$$

Hence, $\vec{B}(u)$ expresses the magnetic field at the origin as produced by the target. Since the target movement direction is a-priori unknown, the magnetometers axes generally do not coincide with $\hat{x}, \hat{y}, \hat{z}$. In order to obtain invariance to the magnetometer attitude regarding the target track we build a magnetic anomaly signal $|\vec{B}(u)|^2$. From (6) we get

$$\left| \vec{B}(u) \right|^2 = \left(\frac{\mu_0}{4\pi R_0^3} \right)^2$$
$$\times \frac{(4m_x^2 + m_y^2 + m_z^2)\, u^2 + 6m_x m_y u + m_x^2 + 4m_y^2 + m_z^2}{(u^2+1)^4}. \qquad (7)$$

III. ORTHONORMAL BASIS FUNCTIONS

A. Signal Decomposition

From (7), we see that three basis functions span the space of $|\vec{B}(u)|^2$

$$\phi_1(u) = \frac{1}{(u^2+1)^4}, \; \phi_2(u) = \frac{u}{(u^2+1)^4}, \; \phi_3(u) = \frac{u^2}{(u^2+1)^4}. \qquad (8)$$

The functions in (8) are linearly independent as proved by a Wronskian matrix with a nonzero determinant

$$\begin{vmatrix} \phi_1 & \phi_2 & \phi_3 \\ \dfrac{d\phi_1}{du} & \dfrac{d\phi_2}{du} & \dfrac{d\phi_3}{du} \\ \dfrac{d^2\phi_1}{du^2} & \dfrac{d^2\phi_2}{du^2} & \dfrac{d^2\phi_3}{du^2} \end{vmatrix}$$
$$= \begin{vmatrix} \dfrac{1}{(u^2+1)^4} & \dfrac{u}{(u^2+1)^4} & \dfrac{u^2}{(u^2+1)^4} \\ \dfrac{-8u}{(u^2+1)^5} & \dfrac{-(7u^2-1)}{(u^2+1)^5} & \dfrac{-2u(3u^2-1)}{(u^2+1)^5} \\ \dfrac{8(9u^2-1)}{(u^2+1)^6} & \dfrac{8u(7u^2-3)}{(u^2+1)^6} & \dfrac{2(21u^4-18u^2+1)}{(u^2+1)^6} \end{vmatrix}$$
$$= \frac{2}{(u^2+1)^{12}} \neq 0. \qquad (9)$$

We strive to build a set of basis functions $g_i(u)$, which are orthonormal, i.e., fulfill the orthogonality and normality conditions

$$\int g_i(u) g_j(u) du = \begin{cases} 1, & i = j \\ 0, & i \neq j \end{cases}. \qquad (10)$$

An orthogonal set is produced using the Gram–Schmidt process in the following manner:

$$\varphi_1(u) = \phi_1(u) = \frac{1}{(u^2+1)^4}$$
$$\varphi_2(u) = \phi_2(u) - \frac{\int \phi_2(\theta)\varphi_1(\theta)d\theta}{\|\varphi_1\|^2} = \frac{u}{(u^2+1)^4}$$
$$\varphi_3(u) = \phi_3(u) - \frac{\int \phi_3(\theta)\varphi_1(\theta)d\theta}{\|\varphi_1\|^2} - \frac{\int \phi_3(\theta)\varphi_2(\theta)d\theta}{\|\varphi_2\|^2}$$
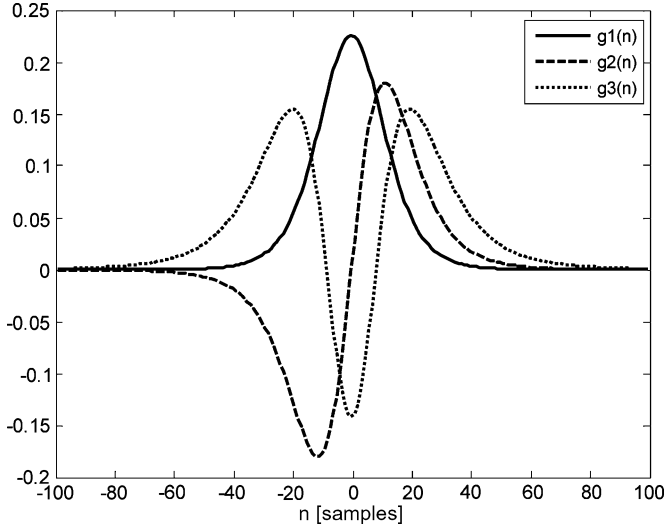$$= \frac{u^2}{(u^2+1)^4} - \frac{0.0769}{(u^2+1)^4}. \qquad (11)$$

Fig. 2.   Three orthonormal basis functions (OBFs).

Afterward, the orthogonal set in (11) is normalized

$$g_1(u) = \frac{0.3899}{(u^2+1)^4}, \quad g_2(u) = \frac{1.4055u}{(u^2+1)^4},$$
$$g_3(u) = \frac{3.1767u^2 - 0.2444}{(u^2+1)^4}. \quad (12)$$

The OBFs $g_1(u), g_2(u), g_3(u)$ are depicted in Fig. 2.

B. Dominant Basis Function

The squared module readings of the referenced magnetometer can be represented as a linear combination of the OBFs using the coefficients $\lambda_1, \lambda_2, \lambda_3$

$$\left| \vec{B}(u) \right|^2 = \left(\frac{\mu_0}{4\pi R_0^3} \right)^2 \sum_{j=1}^{3} \lambda_j g_j(u). \quad (13)$$

From (7), we can express the coefficients $\lambda_1, \lambda_2, \lambda_3$ as a functions of $m_x, m_y, and\ m_z$

$$\lambda_1 = 3.3541m_x^2 + 10.4563m_y^2 + 2.7621m_z^2$$
$$\lambda_2 = 4.2689m_xm_y$$
$$\lambda_3 = 1.2592m_x^2 + 0.3148m_y^2 + 0.3148m_z^2. \quad (14)$$

It can be shown algebraically that for any values of m_x, m_y, and m_z

$$\lambda_1 > 2.7745|\lambda_2|$$
$$\lambda_1 > 2.6641\lambda_3 > 0. \quad (15)$$

Hence, $g_1(u)$ is the most dominant OBF. In the following section we will transform (13) into a discrete form and use it to show that the most dominant OBF should be used to detect the target.

C. Signal Composition

All the three axes of the referenced magnetometer are synchronously sampled with a sampling period of T_s. The ratio R_0/v is defined as the characteristic time τ. Hence, using (3) we replace the continuous variable u by the discrete variable n

$$u = vnT_s/R_0 = nT_s/\tau. \quad (16)$$

We define the normalized coefficients $\gamma_1, \gamma_2, \gamma_3$ using $\gamma_j = (\mu_0/4\pi R_0^3)^2 \lambda_j$ for $j = 1, 2, 3$. As a consequence the squared module output of the referenced magnetometer is represented in a discrete form as

$$s(n) = \sum_{j=1}^{3} \gamma_j g_j(nT_s/\tau) \quad n = -N, -N+1, \ldots, N. \quad (17)$$

We use a moving window of $2N + 1$ samples length for the signal processing. The window length is set according to noise level and τ. Notice that too long sequences tend to pick up extra noise, whereas too short sequences may lose much of the target signal energy.

A target signal $s(n)$ can be decomposed into OBFs, by calculating the normalized coefficients $\gamma_1, \gamma_2, \gamma_3$. Using (10) we get

$$\gamma_j = \sum_{n=-N}^{N} s(n)g_j(nT_s/\tau), \quad j = 1, 2, 3. \quad (18)$$

Since $\gamma_j = (\mu_0/4\pi R_0^3)^2 \lambda_j$ for $j = 1, 2, 3$, it can be shown from (15) that γ_1 is always the largest normalized coefficient. Hence, whenever a target signal is present in the sampled window, the amplitude of $g_1(nT_s/\tau)$ will be larger than the amplitudes of $g_2(nT_s/\tau)$ and $g_3(nT_s/\tau)$. Examining the value of γ_1 detects the presence of the $g_1(nT_s/\tau)$ component and thereby reveals the target. In the following section we will support this argument using eigenvector analysis [13] in order to construct a detector.

IV. DETECTOR

Let us assume that the magnetic anomaly is composed of the target signal $s(n) = [s(-N), s(-N+1), \ldots, s(N)]^T$ contaminated by an additive white Gaussian noise, $w(n) = [w(-N), w(-N+1), \ldots, w(N)]^T$, with a variance of σ^2. We construct a filter $h(n)$ with a finite impulse response (FIR) of $[h(N), h(N-1), \ldots, h(-N)]^T$. The filter $h(n)$ is considered as a detector by setting its coefficients $h(N), h(N-1), \ldots, h(-N)$ to maximize the output when a target signal is present at the input. In order to calculate the SNR, we calculate separately the expected output power for a pure target signal at the input, $E\{(h^Ts)^2\}$, and the expected output power for noise, $E\{(h^Tw)^2\}$. Since $h(n)$ is a FIR filter we can calculate the SNR using

$$\eta = \frac{E\{(h^Ts)^2\}}{E\{(h^Tw)^2\}} = \frac{h^T E\{ss^T\}h}{h^T E\{ww^T\}h}. \quad (19)$$

TABLE I
SIMULATION PARAMETERS

Symbol	Quantity	Value	Units
m	target magnetic moment	0.02	A·m^2
v	target velocity	1	m/sec
CPA	closest proximity approach	3	m
τ	characteristic time	3	sec
T_s	sampling period	0.1	Sec
2N+1	window length	101	samples

Without loss of generality we set to unity the detector gain, $h^T h = 1$. The correlation matrix of Gaussian white noise is $E\{ww^T\} = \sigma^2 I$, where I is the identity matrix. Using the notation $R = E\{ss^T\}$ yields

$$\eta = \frac{h^T R h}{h^T \sigma^2 I h} = \frac{h^T R h}{\sigma^2 h^T h} = \frac{h^T R h}{\sigma^2}. \tag{20}$$

Using eigenvector analysis we show in the Appendix that the functional $h^T R h$ is maximized when h is the eigenvector that corresponds to the maximal eigenvalue of R, $\alpha_{\max}$. In this case, $h^T R h = \alpha_{\max}$, thus

$$\eta_{\max} = \frac{\alpha_{\max}}{\sigma^2}. \tag{21}$$

In what follows, we are going to show that from this point of view, after being sampled in a window, the OBFs in (12) are appropriate candidates for eigenvectors of R. Particularly, $g_1(nT_s/\tau)$ should be used for the detector as it is the most dominant OBF. A numerical analysis was carried out using a computer simulation in order to calculate the eigenvectors. According to the scheme in Fig. 1, a target was moved with a constant velocity along a straight line track passing by a three-axis magnetometer that was placed at the origin. Numerous computer simulations were executed with various parameters values. Table I gives an example of simulation parameters which can reflect a real-world case.

In order to calculate $R = E\{ss^T\}$, we have to obtain a set of sampled signals $\{s\}$, where each sampled signal in the set is associated with a different target magnetic moment orientation. Target magnetic moment orientation is governed by a pair of angles. For each angle we chose a rotation step of 3° and therefore a total of 14 400 target passes were performed. The square module of the referenced magnetometer outputs were collected into a set $\{s\}$. The set of sampled target signals $\{s\}$ is used to calculate R and thereby to obtain the eigenvectors. Here the relations between the three largest eigenvalues are about $33 : 1 : 0.15$, whereas the remaining eigenvalues are much smaller and therefore are neglected. It turned out that the eigenvectors q_1, q_2, q_3 with the largest corresponding eigenvalues and the OBFs g_1, g_2, g_3 are related as follows:

$$\begin{bmatrix} q_1 \\ q_2 \\ q_3 \end{bmatrix} \cong \begin{bmatrix} 1 & 0 & 0.1 \\ 0 & 1 & 0 \\ -0.1 & 0 & 1 \end{bmatrix} \begin{bmatrix} g_1 \\ g_2 \\ g_3 \end{bmatrix}. \tag{22}$$
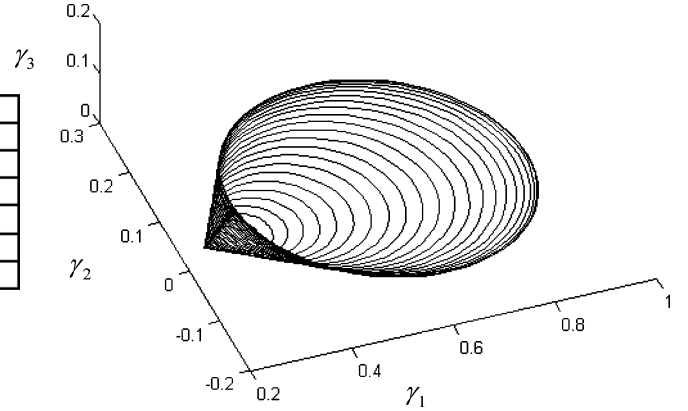

Fig. 3. Values of coefficients $\gamma_1, \gamma_2, \gamma_3$ obtained from decomposition of target signal set.

Ignoring finite precision errors the transformation matrix in (22) is close to the identity matrix I, which implies that practically $q_j = g_j$ for $j = 1, 2, 3$. Hence, we have found that $g_1(nT_s/\tau)$ can be considered as an eigenvector of R with the largest eigenvalue and thereby used as a detector. Using the symmetry of $g_1(nT_s/\tau)$ and ignoring amplification factor the detector is given by

$$h(n) = \left[(nT_s/\tau)^2 + 1 \right]^{-4}. \tag{23}$$

We have also calculated the values of $\gamma_1, \gamma_2, \gamma_3$ on the set $\{s\}$ using (18). Fig. 3 shows the dominance of $g_1(nT_s/\tau)$ since γ_1 is larger than γ_2, γ_3 as expected by (15).

V. EXPERIMENTAL RESULTS

A. Simulation Results

In order to test the proposed detector, we added zero mean Gaussian white noise with $\sigma^2 = 0.002$ nT^2 to the target signal set $\{s\}$. The detector in Fig. 4 was applied for about 10^7 times to the set $\{s\}$, each time with a new noise pattern. Fig. 5 shows the detector output probability density function (PDF) either with or without a target. The threshold value was determined using the Neyman-Pearson criterion [14]. This criterion is useful for achieving maximal detection probability under a constraint on the false alarm rate. Here, we consider false alarm rate as the probability of false alarms per sample period, T_s. The detector receiver operation characteristics (ROC), depicts the resulting detection probability against the false alarm rate. For example, in order to get a false alarm once for 10^5 samples (mean), we use the Neyman-Pearson criterion to find from Fig. 5 a threshold of about 0.07. As a result, a detection probability of about 0.75 is calculated using this threshold as is depicted by the ROC in Fig. 6.

In the described experiment we used an a-priori knowledge of the characteristic time, which in practice can rarely be predicted. Hence, a guess of τ is required or else a multichannel approach should be adopted. Fig. 7 shows the response of the detector as a function of various τ values. The characteristic time was set to 3 s. As expected the detector with $\tau = 3$ s features the highest response. The wide curve in Fig. 7 indicates that only a
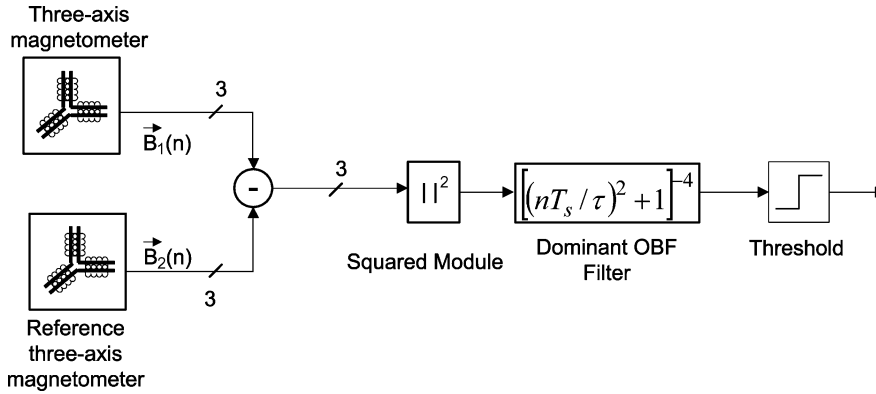
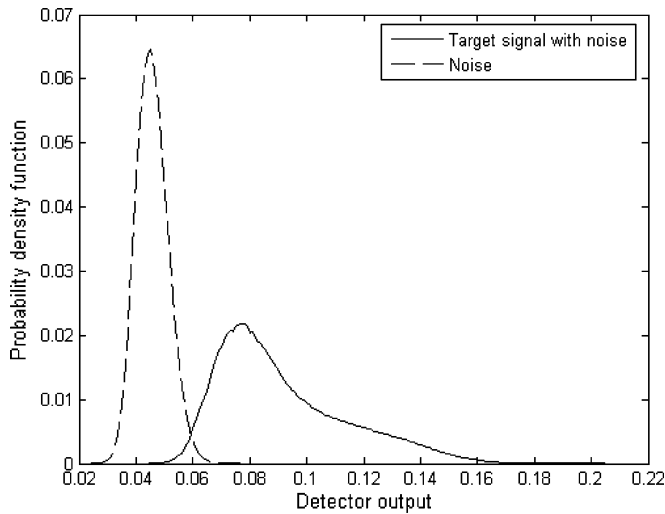Fig. 4. MAD system using a three-axis referenced magnetometer.

Fig. 5. Detector output probability density functions for a zero mean Gaussian white noise with $\sigma^2 = 0.002\ \mathrm{nT}^2$, either with or without a target signal. The target signal was acquired for a target with a magnetic moment of $0.02\ \mathrm{A \cdot m^2}$. The target moved along straight line tracks with a velocity of 1 m/s, passing by the sensor at a CPA of 3 m.
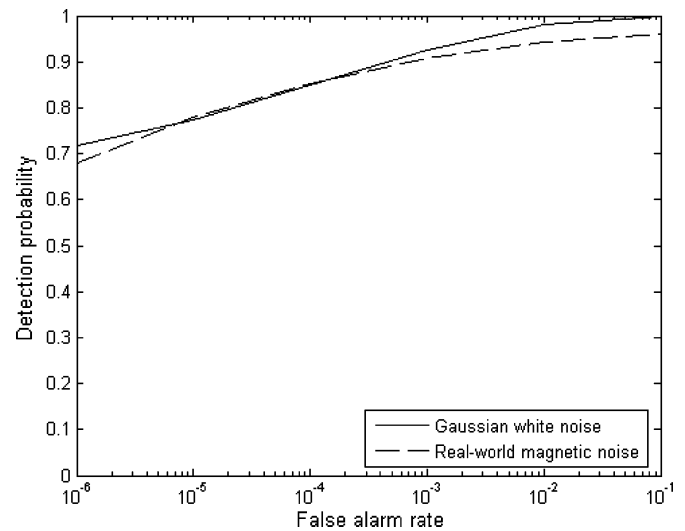

Fig. 6. ROC for the three-axis referenced magnetometer detector. The target signal was acquired for a target with a magnetic moment of $0.02\ \mathrm{A \cdot m^2}$. The target moved along straight line tracks with a velocity of 1 m/s, passing by the sensor at a CPA of 3 m. The target signal was corrupted either by white Gaussian noise or by real-world acquired magnetic noise. In both cases, noise variance is about $0.002\ \mathrm{nT}^2$.

few channels are needed in order to cover possible target characteristic time values.

B. Experiments With Real-World Magnetic Noise

We have tested the ability of the proposed detector to handle real-world signals by applying it to a mixed signal consisting of a simulated magnetic dipole target signal on the background of a real-world magnetic noise. Actually, simulated target signals are very close to acquired target signals but it is much easier to obtain representative statistics. The noise was acquired in a relatively quiet magnetic surrounding, using a LEMI-019 flux-gate magnetometer [15]. The magnetometer intrinsic noise is less than $15.0\ \mathrm{pT}/\sqrt{\mathrm{Hz}}$ at 1 Hz, and the transfer coefficient is 270.0 mV/nT with 5% error. The magnetometer has an internal band-pass-filter with a bandwidth of 0.02–5 Hz. The acquired noise was added to the simulated target signal set $\{s\}$. The set $\{s\}$ was obtained by a computer simulation as explained in the previous section with the parameters given in Table I. Fig. 8 depicts a typical signal contaminated by real-world magnetic noise. Notice that the detector enhances the SNR of the referenced magnetometer squared module output. Fig. 6 shows the
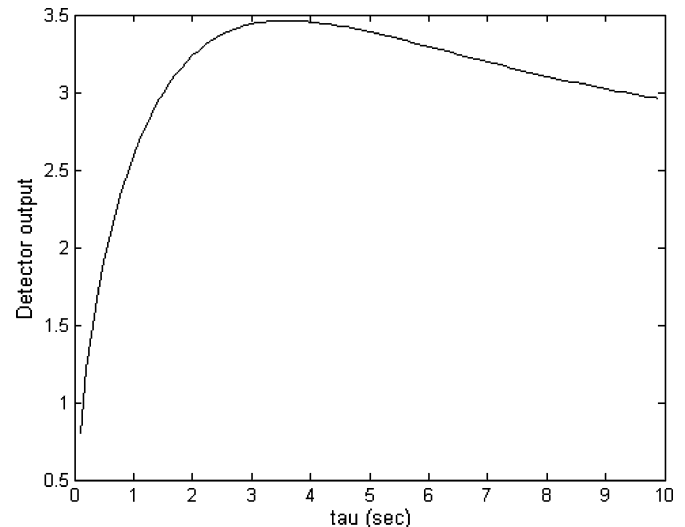

Fig. 7. Typical response of detector for various characteristic time values. The peak coincides with the actual target characteristic time of 3 s.
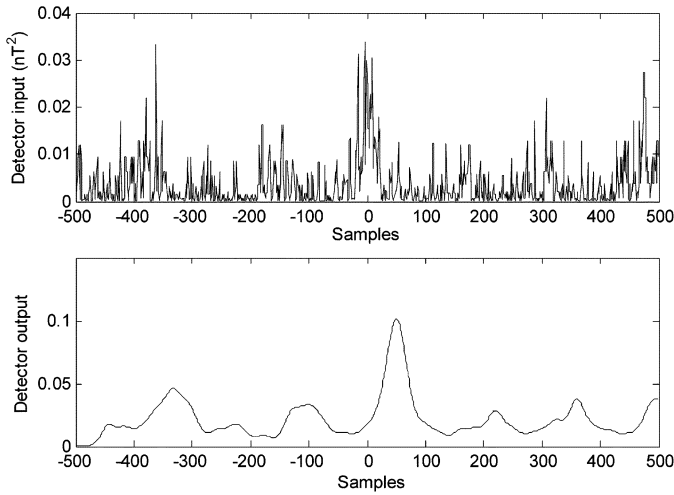
Fig. 8. Record of simulated target signal (in the middle of the window) contaminated by real-world magnetic noise (top). The corresponding detector output is lagged by number of samples equal to detector length (bottom).

Fig. 9. Orthonormal basis functions (OBFs) which are associated with the three largest eigenvalues in case of a parabolic target track.

ROC of the proposed detector for a target with a magnetic moment of 0.02 A $\cdot$ m^2, where the target signal was contaminated by a real-world magnetic noise with an estimated variance of about $\sigma^2 = 0.002$ nT^2. Notice that the detection probability in the case of a real-world magnetic noise is close to the detection probability in the case of white Gaussian noise. The high detection probability even for high level real-world magnetic noise makes the detector very attractive for real-time applications. One of the possible applications is a vehicle detection system [10]. The magnetic moment of a vehicle is determined by its type (private, van, track, etc.), brand (GM, Toyota, Citroen, etc.), orientation, payload and many other parameters. For the purpose of this discussion, a typical magnetic moment of a vehicle is estimated for about 20 A $\cdot$ m^2, which is reasonable according to literature and our experience. When the vehicle is close to the sensor, say about 3 m from the sensor, the generated magnetic field is very strong. In this case, the actual modeling of the vehicle magnetic dipole characteristics is not critical since no detection method is needed. However, for a CPA of about 30 m, according to (1), the magnetic field generated by the vehicle is about the same magnitude as the magnetic field generated by the target with the parameters given in Table I. When the vehicle moves along a straight line with a constant velocity of 10 m/sec, the characteristic time is 3 s, the same characteristic time as in Table I. Thus, a typical signal generated by a vehicle looks as the signal depicted in Fig. 8. In this case, Figs. 5, 6 demonstrate in an adequate manner the vehicle detector performance as well.

VI. FURTHER INVESTIGATION

A. Handling $1/f^\alpha$ Magnetic Noise

A PDF of $1/f^a$ is common for a real-world magnetic noise [16], where in many cases $\alpha \approx 2$. In case of $\alpha \approx 2$, a whitening filter can be realized in time domain as a derivative operator. Applying the whiting filter whitens the noise but also distorts
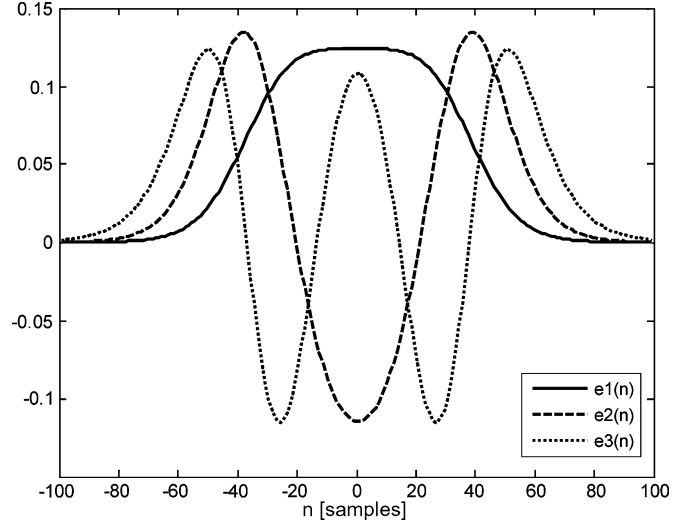
the target signal. Thus, because of whitening the detector should be adopted to detect the derivate of $g_1(u)$

$$\frac{dg_1(u)}{du} = -3.1192u(u^2 + 1)^{-5}. \tag{24}$$

Ignoring amplification and using the antisymmetry of (24), we express the detector in discrete form as

$$h^*(n) = (nT_s/\tau)\left[(nT_s/\tau)^2 + 1\right]^{-5}. \tag{25}$$

Further investigation will focus on testing the detector in (25), and adjusting the detector to efficiently handle a $1/f^a$ magnetic noise with an arbitrary value of α [17].

B. Handling Arbitrary Tracks

The OBFs in (12) were developed for the case of a straight line track, only. The performed analysis is also applicable to a non straight line track, which is practical in many cases. For example we have used the computer simulation to calculate the eigenvectors of a parabolic track. The parabolic track simulates the case where a target approaches the magnetometer and then retreats. Fig. 9 shows the resulting eigenvectors. We have calculated the corresponding eigenvalues for the eigenvectors, and denoted by e_1 as the eigenvector associated with the largest eigenvalue. According to conclusion (21) for the case of a straight line track, we can similarly use e_1 for the detector in case of a parabolic track. Further investigation is required in order to develop and test the method for various track curves.

VII. CONCLUSION

We have developed a detector for revealing the magnetic anomaly of a ferromagnetic target using a three-axis referenced magnetometer. The detector performance was investigated by evaluating its ROC. The results show high detection probability even for low SNR values. The detector simple implementation

as a FIR filter makes it attractive for real-time applications such as intruder detection. Applications of this class are used for perimeter protection, issuing an alarm whenever a person passes by the sensor with a ferromagnetic item.

Further investigation will address adaptation of the detector to the real-world magnetic noise with a PSD of $1/f^a$. We also intend to expend the proposed detection method to handle arbitrary target tracks.

APPENDIX

The proof makes use of principle component analysis [18].

Theorem: Consider a random vector S with a correlation matrix of S is $R = E\{SS^T\}$. Then a unit vector h that maximizes the functional $\Phi(h) = h^T Rh$ is the eigenvector q_{max} that corresponds to the largest eigenvalue α_{max}.

Proof: In order to find the variation of $\Phi(h)$ we add a small perturbation δh to $\Phi(h)$ using

$$\Phi(h + \delta h) = (h + \delta h)^T R(h + \delta h). \quad (A.1)$$

Using the symmetry of the correlation matrix R we can write

$$\Phi(h + \delta h) = h^T Rh + 2(\delta h)^T Rh + (\delta h)^T R(\delta h). \quad (A.2)$$

Neglecting the second order term $(\delta h)^T R(\delta h)$ and using $\Phi(h) = h^T Rh$ we have

$$\Phi(h + \delta h) - \Phi(h) = 2(\delta h)^T Rh. \quad (A.3)$$

We expected that at the maximum point of variation the difference $\Phi(h + \delta h) - \Phi(h)$ will equal to zero

$$(\delta h)^T Rh = 0. \quad (A.4)$$

Since h is a unity vector that satisfies $|h| = 1$ and δh is a small perturbation, we can write, $|h + \delta h| = 1$, which is equivalent to

$$(h + \delta h)^T (h + \delta h) = 1. \quad (A.5)$$

Using $|h| = 1$ and ignoring the second order term $(\delta h)^T \delta h$ we get

$$(\delta h)^T h = 0. \quad (A.6)$$

We will use the Lagrange multiplier α in order to solve $(\delta h)^T Rh = 0$ under the constraint $(\delta h)^T h = 0$

$$(\delta h)^T Rh - \alpha(\delta h)^T h = 0. \quad (A.7)$$

Since $\delta h \neq 0$ we have the eigenvector equation

$$Rh = \alpha h. \quad (A.8)$$

By definition a vector h that satisfies (A.8) is an eigenvector of R, whereas the scalar α is referred to as the corresponding eigenvalue. Thus, substituting for the function $\Phi(h)$ and using $h^T h = 1$, yields

$$\Phi(h) = h^T Rh = h^T \alpha h = \alpha. \quad (A.9)$$

The maximum of $\Phi(h)$ is obtained for the eigenvector that corresponds to the largest eigenvalue, α_{max}.

ACKNOWLEDGMENT

REFERENCES

[1] J. E. McFee and Y. Das, "Locating and identifying compact ferrous objects," *IEEE Trans. Geosci. Remote Sensing*, vol. 28, no. 2, pp. 182–193, Mar. 1990.

[2] E. Paperno, I. Sasada, and E. Leonovich, "A new method for magnetic positioning and orientation tracking," *IEEE Trans. Magn.*, vol. 37, pp. 1938–1940, Jul. 2001.

[3] J. A. Baldoni and B. B. Yellen, "Magnetic tracking system: Monitoring heart valve prostheses," *IEEE Trans. Magn.*, vol. 43, pp. 2430–2432, 2007.

[4] M. Marchetti, L. Cafarella, D. Di Mauro, and A. Zirizzotti, "Ground magnetometric surveys and integrated geophysical methods for solid buried waste detection: A case study," *Ann. Geophys.*, vol. 45, pp. 563–573, 2002.

[5] A. V. Kildishev, J. A. Nyenhuis, and M. A. Morgan, "Multipole analysis of an elongated magnetic source by a cylindrical sensor array," *IEEE Trans. Magn.*, vol. 38, pp. 2465–2467, 2002.

[6] R. J. Blakely, *Potential Theory in Gravity and Magnetic Applications*, 1st ed. Cambridge, U.K.: Cambridge Univ. Press, 1996, pp. 75–79.

[7] P. Ripka, *Magnetic Sensors and Magnetometers*. Boston, MA: Artech House, 2001, pp. 75–120.

[8] P. Ripka, "Advances in fluxgate sensors," *Sens. Actuators A*, vol. 106, pp. 8–14, 2003.

[9] A. Sheinker, N. Salomonski, B. Ginzburg, A. Shkalim, L. Frumkis, and B.-Z. Kaplan, "Network of remote sensors for magnetic detection," in *Proc. 4th Int. Conf. Information Technology: Research and Education (ITRE '06)*, Oct. 2006.

[10] M. O. Kang, B. W. Coi, K. C. Koh, H. J. Lee, and G. T. Park, "Experimental study of a vehicle detector with and AMR sensor," *Sens. Actuators A*, vol. 118, pp. 278–212, 2005.

[11] D. J. Gouws and E. F. Van Der Merwe, The Implementation of a Magnetic SENSOR on a Dynamic Platform [Online]. Available: http://www.hmo.ac.za/old_site/magnetometer_on_dynamic_platform.pdf

[12] B. Ginzburg, L. Frumkis, and B.-Z. Kaplan, "Processing of magnetic scalar gradiometric signals using orthonormalized functions," *Sens. Actuators A*, vol. 102, pp. 67–75, Dec. 2002.

[13] S. Haykin, *Adaptive Filter Theory*, 3rd ed. Englewood Cliffs, NJ: Prentice-Hall, 1996, pp. 181–184.

[14] S. M. Kay, *Fundamentals of Statistical Signal Processing Detection Theory*. Englewood Cliffs, NJ: Prentice-Hall, 1998, pp. 61–75.

[15] LEMI-019 Lviv Centre of Institute of Space Research, Ukraine [Online]. Available: http://www.isr.lviv.ua/lemi019.htm

[16] V. Korepanov and R. Berkman, "Fluxgate magnetometer noise: Theoretic and experimental study," in *Proc. 3rd Biennial Conf. on Measurements for a Sustainable Future (MSA '99)*, 1999, pp. 41–44.

[17] A. Sheinker, A. Shkalim, N. Salomonski, B. Ginzburg, L. Frumkis, and B.-Z. Kaplan, "Processing of a scalar magnetometer signal contaminated by $1/f^a$ noise," *Sens. Actuators A*, vol. 138, pp. 105–111, Jul. 2007.

[18] S. Haykin, *Neural Networks a Comprehensive Foundation*, 2nd ed. Englewood Cliffs, NJ: Prentice-Hall, 1999, pp. 396–400.

Arie Sheinker was born in 1971 in Czernowitz, U.S.S.R (now Ukraine). He received the B.Sc. degree in 1992, and the M.Sc. degree in 2003, both from the Electrical and Computer Engineering Department, Ben-Gurion University of the Negev, Israel. He is pursuing the Ph.D. degree in the Electrical and Computer Engineering Department, Ben-Gurion University of the Negev, and SOREQ Nuclear Research Center. The subject of his thesis is detection and characterization of a magnetic target in noisy environment.

From 1993 to 1999, he was a Communications Systems Engineering Officer in the Israeli Air force.

Lev Frumkis was born in Barnaul, Russia, in 1938. He received the M.Sc. degree in radio-physics and electronics in 1961, the D.Phil. degree in radio-physics in 1967, and the D.Sc. degree in radio-physics in 1989, all from Tomsk State University, Russia.

He served as a Scientist in the Siberian Physics and Technology Institute, Tomsk, where he worked on various electromagnetic problems from 1961 to 1990. He immigrated to Israel in 1991. He served as an Engineer in the Israel aircraft industry from 1991 to 1993. He has been with the Department of Electrical and Computer Engineering, Ben-Gurion University of the Negev, Beer-Sheva, Israel, since 1994, where he is a Research Fellow financed by a Ministry of Absorption Grant. His present research activity is mainly in the field of magnetic shielding and magnetometry.

Boris Ginzburg was born in 1951 in St. Petersburg, Russia. He received the M.Sc. degree in radio physics and electronics from the Technical University of St. Petersburg, Russia, in 1974. He received the Ph.D. degree in physics and mathematics from the Phys.-Techn. Ioffe Institute, St. Petersburg, in 1986.

From 1974 to 1996, he was a Research Scientist with the Geophysical Research Institute, St. Petersburg. During this period, he was engaged in R&D of optical pumping magnetometers for precise measurements of the earth's magnetic field. His experimental investigation of optical pumping phenomena in alkalis and helium resulted in design of new Rb-He and K-He magnetometers with very high metrological features. He headed a research group concerned with elaboration of technological processes for precise magnetic sensors production. He is the head of a research group in Nuclear Research Center SOREQ. His main scientific interests are in the field of precise measurements of the Earth's magnetic field and various magnetic search and detection applications.

Nizan Salomonski was born in 1963 in Haifa, Israel. He received the B.Sc. degree in 1991, the M.Sc. degree in 1994, and the Ph.D. degree in 1999 in mechanical engineering, all of them from The Technion, Israel Institute of Technology, Haifa, Israel.

Since 1998 he has been a member of the American Society for Mechanical Engineering. From 1991 to 1994, he was an Assistant Scientist with the Robotics Laboratory at the Technion. During this period he was engaged in R&D of flexible inflatable articulated robots and control algorithms related to the tool trajectory. From 1994 to 1999, he was a Scientist with the Center for Manufacturing Systems and Robotics (CMSR) at the Technion. During this period he was engaged in R&D of nonparametric algorithms for adaptive disassembly processes and planning mechanisms. He has been with the Nuclear Research Center, SOREQ, since 1999. He is the Head of the R&D Integrated Systems Group in the Nuclear Research Center, SOREQ. His main scientific interests are in the field of nonparametric prediction, detection, and locating via various MAD systems for various applications.

Ben-Zion Kaplan was born in Tel-Aviv, Israel, in 1936. He received the B.Sc. degree (*cum laude*) in 1958 and the M.Sc. degree in 1964, both from The Technion—Israel Institute of Technology, Haifa, Israel, and the D.Phil. degree in electrical engineering from the University of Sussex, Brighton, U.K., in 1971.

From 1961 to 1968, he was a Research Engineer at the Electronics Department (presently the Department of Physics of Complex Systems) in the Weizmann Institute of Science, Rehovot, Israel. From 1968 to 1971, he was with the Inter University Institute of Engineering Control, School of Applied Sciences, University of Sussex. Since 1972, he has been with the Department of Electrical and Computer Engineering of the Ben-Gurion University of the Negev, Beer-Sheva, Israel, where he has been a Professor since 1985 and Professor Emeritus since October 2006. He established the Laboratory for Magnetic and Electronic Systems. He has been the incumbent of the Chinita and Conrad Abrahams-Curiel Chair in Electronic Instrumentation since 1988. In 1992, he was on sabbatical leave in the Department of Physics, University of Otago, Dunedin, New Zealand. He has published more than 130 papers in refereed scientific journals. His main current interests are magnetic and electronic instrumentation, electromechanical devices including magnetic levitators and synchronous machines, nonlinear phenomena in electronic networks and magnetic devices, nonlinear and chaotic oscillations, coupled oscillator systems, multiphase oscillators, magnetometry and its relationship to ELF phenomena, magnetic and electric fields sensors for DC and ULF.

Dr. Kaplan received a prize in the field of applied electronics donated by the Polish-Jewish Ex-Servicemen's Association-London in 1993. The prize was for his achievements in nonlinear electronics and in magnetics. He is a member of the Israeli Committee of URSI and a member of its Metrology Subcommittee.